Caspase-8 activity mediates TNFα production and restricts *Coxiella burnetii* replication during murine macrophage infection

Authors: Chelsea A. Osbron[a], Crystal Lawson[a], Nolan Hanna[a], Heather S. Koehler[a], Alan G. Goodman[a,b#]

[a]School of Molecular Biosciences, College of Veterinary Medicine, Washington State University, Pullman, WA, USA

[b]Paul G. Allen School for Global Health, College of Veterinary Medicine, Washington State University, Pullman, WA, USA

Running title: Caspase-8 regulates *Coxiella burnetii* infection

Keywords: Caspases, tumor necrosis factor, intracellular bacteria, apoptosis, necroptosis

[#]Corresponding Author:
Alan G. Goodman
Washington State University
School of Molecular Biosciences
100 Dairy Rd., BLS 135
Pullman, WA 99164
alan.goodman@wsu.edu

Abstract

Coxiella burnetii is an obligate intracellular bacteria which causes the global zoonotic disease Q Fever. Treatment options for infection are limited, and development of novel therapeutic strategies requires a greater understanding of how *C. burnetii* interacts with immune signaling. Cell death responses are known to be manipulated by *C. burnetii*, but the role of caspase-8, a central regulator of multiple cell death pathways, has not been investigated. In this research, we studied bacterial manipulation of caspase-8 signaling and the significance of caspase-8 to *C. burnetii* infection, examining bacterial replication, cell death induction, and cytokine signaling. We measured caspase, RIPK, and MLKL activation in *C. burnetii*-infected TNFα/CHX-treated THP-1 macrophage-like cells and TNFα/ZVAD-treated L929 cells to assess apoptosis and necroptosis signaling. Additionally, we measured *C. burnetii* replication, cell death, and TNFα induction over 12 days in RIPK1-kinase-dead, RIPK3-kinase-dead, or RIPK3-kinase-dead-caspase-8$^{-/-}$ BMDMs to understand the significance of caspase-8 and RIPK1/3 during infection. We found that caspase-8 is inhibited by *C. burnetii*, coinciding with inhibition of apoptosis and increased susceptibility to necroptosis. Furthermore, *C. burnetii* replication was increased in BMDMs lacking caspase-8, but not in those lacking RIPK1/3 kinase activity, corresponding with decreased TNFα production and reduced cell death. As TNFα is associated with the control of *C. burnetii*, this lack of a TNFα response may allow for the unchecked bacterial growth we saw in caspase-8$^{-/-}$ BMDMs. This research identifies and explores caspase-8 as a key regulator of *C. burnetii* infection, opening novel therapeutic doors.

Introduction

Coxiella burnetii (*C. burnetii*) is a Gram-negative, obligate intracellular bacterial pathogen and the causative agent of the global zoonotic disease query (Q) fever, also known as coxiellosis (1–3). Patients who contract Q fever typically present acute symptoms including fever, fatigue, and muscle aches; however, chronic disease can result in endocarditis and chronic fatigue syndrome, especially in those who are immunocompromised or pregnant (4). There is no widely available vaccine for *C. burnetii*, and current treatments involve antibiotic regimens which can last for over 18 months in chronic cases (5). Additionally, *C. burnetii* exhibits great environmental stability due to its small-cell variant's (SCV) resistance to temperature and desiccation (3). This, combined with its ability to become aerosolized, has led to the labeling of *C. burnetii* as a potential bioterrorism threat (6, 7) and for the United States Center for Disease Control and Prevention (CDC) to categorize *C. burnetii* and select agent (8).

C. burnetii can infect a wide variety of animal hosts, including important livestock species such as sheep, cattle, and goats, as well as ticks, birds, and reptiles. Infected livestock animals are often asymptomatic, but suffer from spontaneous abortions, stillbirths, and weak offspring due to infection (9). Livestock also act as a reservoir from which bacteria is spread to humans, primarily through inhalation of bacteria from contaminated animal urine, feces, blood, milk, and birth products – the last of which has been shown to have high concentrations of bacteria (3, 10, 11). Outbreaks of Q fever in livestock populations have had significant economic consequences. Most well-known is the 2007-2011 Netherlands epidemic, during which disease on dairy goat farms led to estimated costs of 250-600 million euros associated with the over 4,000 human cases and the necessity for large-scale control measures including culling of pregnant animals, breeding restrictions, and strict monitoring of dairy products (12–15).

In general, *C. burnetii* is known to be largely immunologically silent, avoiding or suppressing innate immune signaling during infection (16). Bacterial effectors are vital for sustained suppression of immune signaling and survival of *C. burnetii* within the cell (17–21).

Nevertheless, a recent report by Case *et al.* demonstrated that infection of primary murine bone-marrow-derived macrophages with *C. burnetii* elicits incomplete macrophage M1 polarization and decreased cytokine production during initial stages of infection independently of effector protein secretion (22), highlighting the diverse strategies that *C. burnetii* employs to manipulate its host cell environment.

This lack of a robust immune response can partially be attributed to the bacteria's lifecycle within the cell, as it rapidly forms and replicates within a lysosomal-like compartment called the *Coxiella*-containing vacuole (CCV) (23) shielding its LPS from host immune sensors. While *C. burnetii* can infect a wide range of phagocytic and non-phagocytic cell types including HeLa cells, L929 cells, and macrophages, it has been demonstrated to preferentially infects alveolar macrophages in the lung environment (24–26). Infection of macrophages begins with internalization of the more metabolically silent and resilient SCV into phagosomes by $\alpha_V\beta_3$ integrins (27), followed by the establishment of the CCV through fusion with endosomes, lysosomes, and phagosomes (23). As the pH within the CCV becomes more acidic, *C. burnetii* transitions from its SCV to its more metabolically active and replicative large-cell variant (LCV) (28–32). At this point, the bacteria's Dot/Icm type IVB secretion system (T4SS) begins producing and secreting effector proteins from the CCV, of which over 140 candidates have been identified (33, 34). These effectors manipulate an array of host signaling pathways including, but not limited to, apoptosis, autophagy, inflammasome activation, transcription, and translocation (35). After approximately six days of growth within the cell, *C. burnetii* begins transitioning back into its SCV, such that both SCV and LCV can be found within the large CCV (29). At this point, the bacteria can spread to other cells through egress methods that have until recently been unknown, but are now known to involve host cell apoptosis (36).

Programmed cell death signaling, once limited to the ideas of apoptosis and necrosis (37), is now a complex area of research encompassing a plethora of other modes of regulated cell death such as necroptosis, pyroptosis, ferroptosis, and PANoptosis, the latter of which

96 highlighting that the path to cell death is not a straight line and that signaling molecules in these
97 pathways often have multiple roles (38, 39). For the purposes of this work, however, we will focus
98 on apoptosis and necroptosis. Apoptosis is non-lytic, non-inflammatory, and can be divided into
99 two types: intrinsic and extrinsic (40). Canonically, the intrinsic, or mitochondrial, pathway is
100 triggered by cellular stress such as ROS, ER stress, or UV damage, and is regulated by
101 mitochondrial release of cytochrome c and activation of caspase-9 (41–43). Induction of the
102 extrinsic pathway, in contrast, is the result of activation of death receptors such as tumor necrosis
103 factor alpha (TNFα) receptors (TNFRs) (40, 44). This leads to recruitment of death-inducing
104 signaling complex (DISC) components to the TNFRs, notably TNFR-associated death domain
105 (TRADD), TNFR-associated factors (TRAFs), receptor-interacting protein kinase 1 (RIPK1), and
106 caspase-8 (45–48). This in turn leads to caspase-8 activation. Following caspase-9 or -8
107 activation, the two pathways converge, as both caspases activate caspase-3 to bring about
108 apoptosis (49–51).

109 Not only does caspase-8 induce apoptosis, but it also inhibits necroptosis (52, 53).
110 Apoptosis and necroptosis are, in some ways, opposing modes of programmed cell death (54).
111 Apoptosis, on the one hand, is a slower, non-lytic, and non-inflammatory process; on the other
112 hand, necroptosis is rapid, lytic, and highly inflammatory. However, both forms of cell death can
113 be activated by TNFα. Specifically, if, following TNFR activation, caspase-8 is inhibited such that
114 extrinsic apoptosis cannot occur, RIPK1 can interact with RIPK3 leading to phosphorylation of
115 pseudokinase mixed lineage kinase domain-like protein (MLKL) (55–57). Phosphorylated MLKL
116 (p-MLKL), then causes pore formation in the cell membrane and subsequent cell lysis (58).

117 Past work regarding host cell death during *C. burnetii* infection has primarily focused on
118 intrinsic apoptotic signaling mediated by caspase-9 and the mitochondria and what methods the
119 bacteria uses to subvert and control it (59). Indeed, several effector proteins have been identified
120 which inhibit intrinsic apoptosis during early infection (60–66), and bacterial activation of apoptosis
121 at late stages of infection has been documented (36). In contrast, while it has been shown that *C.*

burnetii prevents extrinsic, caspase-8-mediated apoptosis induction at early stages of infection (67), the mechanisms by which this inhibition is accomplished and the significance to infection remain unknown. To address the knowledge gap surrounding bacterial interactions with cell death beyond intrinsic apoptosis, we investigated the interactions between *C. burnetii* and caspase-8. The focus of this study is on bacterial manipulation of caspase-8 signaling and the role of caspase-8 during *C. burnetii* infection, with an emphasis on consequences for bacterial replication, cell death induction, and cytokine signaling.

Results

C. burnetii inhibits TNFα-mediated caspase-8 activation

While *C. burnetii* has been documented to inhibit both intrinsic and extrinsic apoptosis, mechanistic details have only been investigated for bacterial manipulation of the intrinsic pathway (68). To determine if *C. burnetii* inhibits extrinsic apoptosis at the caspase-8 level, we treated *C. burnetii*-infected THP-1 macrophage-like cells with TNFα and cycloheximide (CHX) to induce extrinsic apoptosis. Briefly, differentiated THP-1 cells (seeded at 10^6 cells/well in 12 well plates) were incubated with mCherry-expressing NMII *C. burnetii* (mCherry-*C. burnetii*) at a multiplicity of infection (MOI) of 25 GE/cell for 24 h, then washed to remove non-internalized bacteria (1 day post infection). At 3 days post infection (DPI), cells were pre-treated with 10 μg/mL CHX for 4 h, then incubated for 16 h with 20 ng/mL human TNFα.

Morphologically, *C. burnetii*-infected cells had an enlarged appearance consistent with harboring large CCVs and showed abundant mCherry signal (Fig 1A). While both infected and uninfected cells treated with TNFα/CHX visually had some cells that appeared to be dead or dying, by western blot it was obvious that *C. burnetii* infection had an inhibitory effect on cell death. Namely, we found that *C. burnetii* significantly reduce the cleavage of caspase-9, caspase-8, caspase-3, and PARP following TNFα treatment (Fig 1B). Previous work has demonstrated

147 bacterial-inhibition of caspase-9, caspase-3, and PARP; however, this is the first report to our
148 knowledge of caspase-8 inhibition by *C. burnetii* during extrinsic apoptosis or otherwise.
149 Furthermore, there was a marked upregulation of $FLIP_L$ protein levels in our infected cells
150 (Fig 1B-C), correlating with findings by Voth *et al.* regarding *cflip* mRNA upregulation (67). As
151 FLIP is an inhibitor of caspase-8, this upregulation could be one way that *C. burnetii* inhibits
152 caspase-8. Nevertheless, there was a significant reduction in FLIP levels following TNFα
153 treatment regardless of infection, rendering it possible, if not likely, that FLIP upregulation is not
154 the only method *C. burnetii* utilizes to prevent caspase-8 activation.
155
156 **_C. burnetii_ infection sensitizes L929 cells to necroptosis**
157 Caspase-8 is not only an initiator of apoptosis, but also a vital inhibitor of necroptosis.
158 Indeed, the knockout of caspase-8 in mice is embryonically lethal due to an over-activation of
159 RIPK3 leading to necroptosis (69). Therefore, by inhibiting caspase-8, *C. burnetii* could
160 inadvertently trigger necroptotic signaling during infection. To investigate this possibility, we
161 infected L929 cells (seed at $5x10^4$ cells/well in 24 well plates) with mCherry-*C. burnetii* at an MOI
162 of 600 GE/cell, incubating cells with bacteria for 24 h then washing to remove non-internalized
163 bacteria (1 DPI). As L929 cells are non-phagocytic, we observed a much lower rate of infectivity
164 than in our macrophage cells, which is what led to the usage of a higher MOI here. At 3 and 6
165 DPI, L929 cells were treated with the pan-caspase inhibitor Z-VAD-FMK (ZVAD) for 30 minutes,
166 followed by treatment with mouse TNFα for 3 h.
167 Phenotypically, both infected and mock-infected cells at 3 and 6 DPI which were treated
168 with TNFα/ZVAD appeared rounded and swollen, consistent with necroptosis (Fig 2A and D).
169 Additionally, we found that the phosphorylation of RIPK1, RIPK3, and MLKL in response to
170 TNFα/ZVAD treatment was amplified in our infected cells at both 3 (Fig 2B) and 6 DPI (Fig 2E).
171 Indeed, in the case of MLKL, densitometry analysis revealed that this phosphorylation was
172 approximately 1.5-fold and 3-fold higher in *C. burnetii*-infected cells at 3 and 6 DPI, respectively

(Fig 2C and F). These data indicate that bacterial infection intensifies necroptosis in L929 cells, notably more at 6 DPI than at 3 DPI, suggesting a relationship between the stage of infection and the sensitivity of infected cells to necroptosis.

Interestingly, we neither observed dying cells nor detected phosphorylation of RIPK1, RIPK3, or MLKL in our infected cells treated with TNFα alone (Fig 2B), indicating that the caspase inhibition by *C. burnetii* is not as potent as our pharmacological inhibition and may not be substantial enough to result in cell death during typical cellular conditions. Thus, we concluded that *C. burnetii* infection sensitizes L929 cells to necroptosis when induced but does not appear to induce it on its own at these timepoints.

$Ripk3^{K51A/K51A}Casp8^{-/-}$ BMDMs have increased *C. burnetii* replication at late stages of infection

Thus far, we have documented for the first time that *C. burnetii* (1) inhibits caspase-8 to prevent extrinsic apoptosis in THP-1 cells and (2) sensitizes L929 cells to necroptosis. Nevertheless, it remains to be seen if caspase-8 or RIPK activity is an important aspect of the immune response to *C. burnetii* infection outside of situations of pharmacological induction. To determine whether caspase-8, RIPK1, or RIPK3 activity restrict *C. burnetii* replication, we utilized BMDMs derived from femurs of C57BL/6J wild-type (WT), $Ripk1^{K45A/K45A}$ (RIPK1-kinase-dead, R1KD) (70), $Ripk3^{K51A/K51A}$ (RIPK3-kinase-dead, R3KD) (71), and $Ripk3^{K51A/K51A}Casp8^{-/-}$ (RIPK3-kinase-dead-caspase-$8^{-/-}$, R3KDCasp$8^{-/-}$) (71) mice. Notably, these kinase-dead BMDMs are still able to produce RIP1 and RIP3 proteins, but those kinases are unable to function enzymatically. Furthermore, since the knockout of caspase-8 on its own is embryonically lethal in mice (69), both WT and R3KD BMDMs serve as controls for the R3KDCasp$8^{-/-}$ BMDMs.

We infected these BMDMs (seeded at 10^5 cells/well in 12 well plates) with mCherry-*C. burnetii* at an MOI of 300 GE/cell by incubating cells with bacteria for 1 hour in media containing 2% FBS, followed by thorough washing to remove non-internalized bacteria (0 DPI). To facilitate

199 infection, cells and bacteria were centrifuged at 300 rcf for 10 minutes at the start of the 1 hour
200 incubation. To quantify bacteria load, we measured bacterial genome equivalents (GE) at 3, 6, 9,
201 and 12 DPI via quantitative real-time polymerase chain reaction (qPCR) targeting the *C. burnetii*
202 *dotA* gene.(29) To further probe the course of infection in these cells, we also assessed the
203 percentage of cells which were infected. For these experiments, BMDMs were seeded at 2 x 10^4
204 cells/well in 96 well plates and were infected as described above with mCherry-*C. burnetii*. At 6
205 and 12 DPI, cells were stained with Hoechst to label nuclei and the percentage of cells which
206 were also mCherry-positive was quantified.

207 *C. burnetii* was able to productively infect and replicate within all the genotypes tested (Fig
208 3A), and our qPCR analysis revealed that, while bacterial load was not different during early
209 stages of infection, by 12 DPI there was significantly more bacteria in BMDMs lacking caspase-8
210 than in any other genotype (Fig 3B). In fact, we detected a ~2.5-fold increase in the amount of *C.*
211 *burnetii* in the infected R3KDCasp8$^{-/-}$ BMDMs compared to the WT and R3KD BMDMs, and a
212 ~1.5-fold increase in the amount compared to the R1KD BMDMs. This increased replication in
213 R3KDCasp8$^{-/-}$ BMDMs was accompanied by an approximately 2-fold increase in the percent of
214 cells which harbored bacteria compared to all other genotypes (Fig 3C). These results support
215 the role of caspase-8 in restricting *C. burnetii* replication and spread, specifically during late-stage
216 infection. Moreover, as there was not higher bacterial load in the R1KD and R3KD cells compared
217 to the WT, it is unlikely that necroptosis is a key regulator of NMII *C. burnetii* replication in BMDMs.
218
219 **Cell death is reduced in *Ripk3*$^{K51A/K51A}$ and *Ripk3*$^{K51A/K51A}$*Casp8*$^{-/-}$ BMDMs throughout *C.**
220 ***burnetii* infection**
221 Caspase-8 has multiple roles within the cell and is a key regulator of cell death pathways
222 including apoptosis, necroptosis, and pyroptosis (72). This, combined with the importance of cell
223 death signaling pathways to *C. burnetii* infection (59), renders it possible that disruption of cell
224 death regulation in the caspase-8-negative BMDMs is responsible for the increased susceptibility

to infection. To determine if cell death levels were altered in R3KDCasp8$^{-/-}$ BMDMs during *C. burnetii* infection, we assessed cytotoxicity by SYTOX staining. For these experiments, BMDMs were seeded and infected in 96-well plates as in Fig 3 with mCherry-*C. burnetii*. At 6 and 12 DPI, cells were stained with SYTOX to identify dying cells and stained with Hoechst to label nuclei, and the percentage of cells which were SYTOX-positive was calculated.

We found that, at 6 (Fig 4A) and 12 DPI (Fig 4B), both R3KD and R3KDCasp8$^{-/-}$BMDMs had significantly reduced cytotoxicity compared to WT. In contrast, R1KD BMDMs only had reduced cytotoxicity compared to WT at 12 DPI. In the case of the R3KD cells, the decrease in cell death throughout infection is likely due to the lack of RIPK3-mediated necroptosis. While the R3KDCasp8$^{-/-}$ BMDMs lack both RIPK3-mediated necroptosis and caspase-8-mediated apoptosis, the combined loss of both pathways unexpectedly did not amplify the loss of cytotoxicity. In the R1KD cells, while there is a lack of RIPK1-mediated necroptosis, necroptosis via other pathways should remain unaltered as RIPK3 is still active. Furthermore, though the scaffolding roles of RIPK1 in regulated apoptosis should be preserved in the R1KD cells, it is possible that some dysregulation of apoptosis occurs (73–75). Thus, the decreased cell death in the R1KD BMDMs at 12 DPI may indicate that RIPK1-mediated cell death is induced at late stages of infection. In contrast, we found that cell death due to infection was not dependent on RIPK1 kinase activity at 6 DPI. Overall, we concluded that the activity of RIPK1 and RIPK3 are both key factors in mounting a cell death response to *C. burnetii* infection in BMDMs, with RIPK1-mediated cell death playing a more important role at late stages of infection compared to early stages. Additionally, our results suggest that caspase-8 plays either a limited role in the cell death response to infection, or one that is dependent on RIPK3.

Ripk3$^{K51A/K51A}$*Casp8*$^{-/-}$ BMDMs have an attenuated TNFα response to *C. burnetii* infection

Beyond apoptosis and necroptosis, caspase-8 plays a key scaffolding role during TNFα-mediated cytokine signaling (72). Therefore, to further discern what signaling changes are

occurring in our R3KDCasp8$^{-/-}$ BMDMs that could allow for increased *C. burnetii* growth, we investigated TNFα induction during infection by quantitative real-time reverse-transcription PCR (qRT-PCR) and enzyme-linked immunosorbent assay (ELISA). For qRT-PCR experiments, BMDMs were seeded at 10^5 cells/well in 12 well plates and were lysed in TRIzol at 6 and 12 DPI. For ELISA experiments, BMDMs were seeded at 2 x 10^4 cells/well in 96 well plates and cell-free supernatant was collected at 12 DPI. In both sets of experiments, BMDMs were infected as in Fig 3 with mCherry-*C. burnetii*.

Our qRT-PCR analysis showed a reduction of *tnfα* expression in infected R3KDCasp8$^{-/-}$ BMDMs compared to WT at 6 DPI and an even greater reduction compared to both the WT and R3KD BMDMs at 12 DPI. Quantification of TNFα secretion via ELISA at 12 DPI supported this finding, where we found a moderate reduction in TNFα concentration in cell-free supernatant of R3KD BMDMs and a large reduction in R3KDCasp8$^{-/-}$ cells. Together, these data indicate that, without caspase-8, BMDMs initiate a highly attenuated TNFα response to *C. burnetii* infection in BMDMs. As TNFα has been associated with restricting *C. burnetii* growth within cells (76–79), it is possible that this lack of TNFα production in R3KDCasp8$^{-/-}$ BMDMs leads to increased bacterial replication in these cells.

Discussion

In this study, we provide one of the first reports for the role of caspase-8 during *C. burnetii* infection. Using THP-1 and L929 infection models, we demonstrated that *C. burnetii* inhibits caspase-8 activation during TNFα-mediated apoptosis and sensitizes cells to TNFα-mediated necroptosis. We also showed that caspase-8 restricts *C. burnetii* replication, as BMDMs lacking caspase-8 showed increased bacterial load and percent infection by 12 DPI. The increased bacterial spread in caspase-8-negative cells is likely connected to the increased bacterial replication, as it was recently discovered that *C. burnetii* egress is dependent on bacterial load (36). This higher susceptibility of caspase-8 deficient BMDMs to *C. burnetii* during late stages of

277 infection also corresponded with decreased TNFα production and lower cytotoxicity, though the
278 latter appeared to also be tied to the loss of RIPK3 activity and is thus not likely to be the sole
279 contributing factor. As TNFα has been associated with the control of *C. burnetii*, it is possible that
280 the lack of a TNFα response in our caspase-8-negative cells allowed for the unchecked bacterial
281 growth.

282 During infection, *C. burnetii* heavily manipulates the host cell environment to control
283 apoptosis and several anti-apoptotic effector proteins have been identified (59). Until now,
284 however, the ability of *C. burnetii* to inhibit caspase-8 was unknown, despite its key role in
285 regulating not only apoptosis, but also necroptosis and pyroptosis (72). Previously, it was shown
286 that TNFα-induced apoptosis is inhibited by *C. burnetii* (64, 67) and that the *C. burnetii* effector
287 CaeA is able to prevent apoptosis at the executioner caspase-3 level (64), but whether bacterial
288 manipulation of extrinsic apoptosis is limited to downstream steps or also includes upstream
289 signaling had not been investigated. We have demonstrated that, indeed, caspase-8 activation
290 and subsequent apoptosis is prevented by *C. burnetii* infection, extending past research and
291 highlighting the extent to which *C. burnetii* is able to interfere with host cell signaling. Additionally,
292 we were able to establish that the caspase-8 inhibitor cFLIP is over-expressed in *C. burnetii*-
293 infected cells, validating and expanding findings by Voth *et al.* which showed increased cFLIP
294 mRNA levels during infection (67). This over-expression likely contributes to bacterial inhibition of
295 caspase-8, though it is also possible, if not probable, that effector proteins are involved, as with
296 *C. burnetii* inhibition of other apoptotic caspases (60, 65, 64). An effector screen, as well as a
297 mutant library screen, would be beneficial in determining which effector proteins or other bacterial
298 factors, known or unknown, are involved in the inhibition of caspase-8.

299 As discussed earlier, caspase-8 sits at the nexus of multiple cell death pathways, and
300 caspase-8 inhibition is a critical step in induction of necroptosis (54). Because of its inhibition of
301 caspase-8, we theorized that cells infected with *C. burnetii* would be susceptible to necroptotic
302 death. Indeed, we found that infected L929 cells treated to induce necroptosis had ~3-fold more

MLKL phosphorylation than uninfected cells at 6 DPI. This vulnerability to necroptosis is a vital piece of information, as it suggests a possible blind-spot in the anti-cell death regime of *C. burnetii*. It is possible that, similarly to its approach to pyroptosis and in contrast to its approach to apoptosis, *C. burnetii* primarily utilizes a stealth strategy as opposed to a defensive one to avoid necroptotic cell death (24, 78, 80–82). However, whether necroptosis results in the killing of bacteria within the cell or if it is a mechanism by which *C. burnetii* spread can occur remains to be seen. The effect of necroptosis on *C. burnetii* is likely also dependent on the stage of infection. If the CCV is predominately composed of LCV bacteria, for instance, necroptosis may have a higher bactericidal effect than if the CCV predominately contains the more resistant SCV bacteria.

Surprisingly, though *C. burnetii* infection rendered L929 cells more vulnerable to necroptosis, loss of RIPK3 kinase activity, and thus the ability to undergo necroptotic cell death, did not result in a difference in susceptibility of BMDMs to *C. burnetii*. This is intriguing, as Ripk3$^{-/-}$ BMDMs have recently been found to have higher bacterial loads by 7 DPI compared to WT BMDMs, a phenotype lost in Ripk3$^{-/-}$Caspase-8$^{-/-}$ BMDMs (83). These data, combined with our own bacterial replication data, suggest that RIPK3 has significance to combatting *C. burnetii* infection independent of its kinase activity but dependent on caspase-8.

Despite the apparent dispensability of RIPK1 and RIPK3 kinase activity to controlling *C. burnetii* replication, we did see an approximately 2-fold and 3-fold increase in cell death by 6 and 12 DPI, respectively, in infected WT BMDMs which was dependent on RIPK1 activity at 12 DPI and on RIPK3 activity at both 6 and 12 DPI. These results implicate necroptotic machinery in cell death from infection. Overall, our bacterial replication and cell death assays suggest that, while necroptotic signaling components are involved in cell death during infection, they are dispensable to controlling or supporting *C. burnetii* replication.

Interestingly, our data also suggest that RIPK1 may have more involvement in cell death at late stages of infection, possibly in relation to increased (but still moderate) TNFα secretion at these time points. Additionally, while RIPK1 kinase activity is well-known as an inducer of

329 necroptosis alongside RIPK3, the kinase activity of RIPK1 has also been associated with
330 apoptosis regulation (73–75). Thus, it is possible that multiple cell death pathways are
331 dysregulated in the R1KD cells. This nuanced role of RIPK1 in cell death at different timepoints
332 during *C. burnetii* infection should be further probed to assess if and how its activity could be
333 leveraged therapeutically.

334 The combined loss of caspase-8 and RIPK3 activity surprisingly did not result in a further
335 decrease to cell death, despite our observed importance of caspase-8 to TNFα production. The
336 mechanisms by which TNFα is able to control *C. burnetii* infection is an ongoing area of research,
337 with past work showing that TNFα is vital to IFNγ-mediated control of *C. burnetii* (76, 77), and
338 more recent studies implicating TNFα in restricting bacterial replication following toll-like receptor
339 (TLR) activation (78) and in hypoxic conditions (79). Mechanistically, Boyer *et al*. found that TNFα
340 restriction of *C. burnetii* replication in BMDMs involves IRG1-itaconate signaling (83), a pathway
341 which has also been implicated by Kohl *et al*. (84). While TNFα treatment appears to be able to
342 control *C. burnetii* in cells lacking caspase-8,(83) this study adds caspase-8 to the mix of
343 endogenous TNFα regulators during infection. Further characterizing the role that caspase-8
344 plays within the mechanisms of TNFα-mediated control of *C. burnetii*, for cell death signaling and
345 otherwise, will enhance our ability to harness the innate immune system to fight infection.

346 Moreover, this work, combined with past research documenting the increased disease
347 severity in *C. burnetii*-infected mice deficient in TNFα (85), raises the possibility that patients
348 taking TNFα blockers may be particularly vulnerable to Q fever. Following the outbreak in the
349 Netherlands, one group attempted to address this very question by examining *C. burnetii*
350 seroprevalence and chronic disease in patients with rheumatoid arthritis (RA) who were on anti-
351 TNFα therapy (86). While patients with RA had a much higher prevalence of chronic Q fever
352 overall (87), convincing conclusions were unable to be drawn regarding the risk of anti-TNFα
353 therapies in particular due to their limited sample size. Recently, the potential for selectively
354 inhibiting or activating TNFR1 and TNFR2 to treat inflammatory and degenerative diseases as an

alternative to broad inhibition of both receptors was reviewed by Fischer *et al*. (88). The differential roles of TNFR1 and TNFR2 in the context of *C. burnetii* infection have not, to our knowledge, been explored, though TNFR2 upregulation in monocytes has been associated with Q fever endocarditis (89). This line of research should be further pursued to conclusively determine the connection between anti-TNFα therapy and Q fever risk.

The importance of caspase-8 during pathogenic infection has been documented in the context of many pathogenic species, including *Yersinia* (90–93) and herpes simplex virus 1 (HSV1) (94–96). In the case of *Yersinia*, the effector protein YopJ inhibits transforming growth factor β-activated kinase 1 (TAK1) and IKKβ (97–100), leading to RIPK1-dependent induction of caspase-8-mediated cleavage of gasdermin D (GSDMD) to induce pyroptosis and secretion of IL-1β (90–93). Our investigation of the relationships between caspase-8 and *C. burnetii* is a vital step in the path to understanding the significance of programmed cell death signaling to not only *C. burnetii* infection, but also to other pathogens, obligate intracellular bacteria or not, which interact with these pathways. As such, a deeper exploration of the mechanisms behind our findings will aid in the development of novel therapeutic strategies to improve animal and human health.

Methods

Cell Culture

Human THP-1 monocytes were maintained at a density between $3x10^5$ and 10^6 cells/mL in 1x RPMI 1640 (Gibco 11875093) supplemented with 10% FBS (Cytiva Hyclone SH30070.03HI), 1 mM sodium pyruvate (Gibco 11360070), 10 mM HEPES (Gibco 15630106), and 50 μM beta-mercaptoethanol (Gibco 21985023), and 1x antibiotic-antimycotic (Gibco 15240062) at 37°C in 5% CO_2. For differentiation into macrophage-like cells using phorbol 12-myristate 13-acetate (PMA; Sigma-Aldrich P1585), THP-1 monocytes were seeded in media

containing 100 nM PMA. After 24 h, PMA-containing media was replaced with media containing no PMA, and cells were allowed to rest for 24 h prior to infection.

Mouse L929 cells were maintained in 1x DMEM, high glucose (Gibco 11965092) supplemented with 10% FBS (Atlas Biologicals EF-0500-A) and 1x antibiotic-antimycotic (Gibco 15240062) at 37°C in 5% CO_2.

Primary murine bone marrow macrophages (BMDMs) were derived from bone marrow cells isolated from femurs of C57BL/6J WT, *Ripk1*$^{K45A/K45A}$, *Ripk3*$^{K51A/K51A}$, and *Ripk3*$^{K51A/K51A}$*Casp8*$^{-/-}$ mice (70, 71). Briefly, bone marrow cells were differentiated for 7-10 days using 1x DMEM, low glucose, pyruvate (Gibco 11885084) supplemented with 10% FBS (Cytiva Hyclone SH30070.03HI), 30% L929 conditioned media (LCM), and 1x antibiotic-antimycotic (Gibco 15240062) at 37°C in 5% CO_2, and 1/2 volume of media was replaced every 3 days.

Bacterial stock and infection

mCherry expressing *C. burnetii* NMII (clone 4 RSA439) (mCherry-*C. burnetii*) was grown in Acidified Citrate Cysteine Medium 2 containing tryptophan (ACCM-2 + tryptophan) as previously described (101–103). *C. burnetii* bacterial stocks were quantified by quantitative polymerase chain reaction (qPCR) to measure genome equivalents (GE) (29, 104).

Differentiated THP-1 cells were washed 2x with incomplete 1x RPMI 1640 (Gibco 11875093) then incubated with mCherry-*C. burnetii* at a MOI of 25 GE/cell for 24 h in 1x RPMI 1640 supplemented with 10% heat-inactivated FBS (Cytiva Hyclone SH30070.03HI), 1 mM sodium pyruvate (Gibco 11360070), 10 mM HEPES (Gibco 15630106), and 50 µM beta-mercaptoethanol (Gibco 21985023). Following infection, THP-1 cells were washed twice with incomplete 1x RPMI 1640 to remove extracellular bacteria (1 DPI) and maintained in 1x RPMI 1640 supplemented with 10% FBS, 1 mM sodium pyruvate, 10 mM HEPES, and 50 µM beta-mercaptoethanol, with 1/2 volume of media replaced daily.

L929 cells were washed 2x with incomplete 1x DMEM, high glucose (Gibco 11965092) then incubated with mCherry-*C. burnetii* at a MOI of 600 for 24 h in 1x supplemented with 10% FBS (Atlas Biologicals EF-0500-A) with a 30 minutes spin at 300 rcf. Following infection, L929 cells were washed 2x with incomplete 1x DMEM to remove extracellular bacteria (1 DPI) and maintained in 1x DMEM supplemented with 10% FBS.

Differentiated BMDMs were washed twice with incomplete 1x DMEM, low glucose, pyruvate (Gibco 11885084) then incubated with mCherry-*C. burnetii* at a MOI of 300 GE/cell for 1 h in 1x DMEM supplemented with 2% FBS (Cytiva Hyclone SH30070.03HI) with a 10 minutes spin at 300 rcf. Following infection, BMDMs were washed twice with incomplete 1x DMEM to remove extracellular bacteria (0 DPI) and maintained in 1x DMEM supplemented with 10% FBS and 10% LCM, with 1/2 volume of media replaced daily.

Cell Death Induction

For extrinsic apoptosis induction in THP-1 macrophage-like cells, cells were pre-treated with 10 µg/mL cycloheximide (CHX; Selleckchem S7418) for 4 h, then treated with 20 ng/mL human tumor necrosis factor alpha (TNFα; Sigma-Aldrich H8916) for 16 h.

For necroptosis induction in L929 cells, cells were pre-treated with 50 µM Z-VAD-FMK (Calbiochem/Sigma-Aldrich 627610) for 30 minutes followed by 3 h treatment with 20 ng/mL mouse TNFα (Calbiochem/Sigma-Aldrich 654245).

Immunoblotting

Protein extracts were prepared either by lysing cells directly in 2x Laemmli buffer (0.125 M Tris-HCL pH 6.8, 4% SDS w/v, 20% glycerol, 0.004% bromophenol blue w/v, 10% beta-mercaptoethanol) (for necroptosis experiments in L929 cells and BMDM experiments) or by lysing cells in RIPA buffer (25 mM Tris-HCl pH 7.6, 150 mM NaCl, 1 mM EDTA, 1% NP-40, 1% sodium deoxycholate, 0.1% SDS, 1mM Na3VO4, 1 mM NaF, 0.1 mM PMSF, 10 µM aprotinin, 5 µg/mL

leupeptin, 1 µg/mL pepstatin A) followed by dilution in 2x Laemmli buffer (for extrinsic apoptosis experiments in THP-1 cells). After mixing with Laemmli buffer, samples were heated for 5-10 minutes at 95°C and centrifuged for 5 minutes at 12,000 rcf. Samples were separated by SDS-PAGE using 10% or 15% acrylamide gels, followed by transfer onto 0.45 µm PVDF membranes (Immobilon/Sigma-Aldrich IPVH00010). Membranes were blocked for 30 minutes at room temperature with 5% nonfat dry milk (Lab Scientific/VWR M0841) or 5% BSA (ThermoFisher BP9706) in Tris-buffered saline (50 mM Tris-HCl pH 7.5, 150 mM NaCl) containing 0.1% Tween-20 (ThermoFisher BP337). Membranes were then labeled with primary antibody (see detailed list of antibodies below) overnight rocking at 4°C, then labeled with either anti-rabbit IgG-HRP conjugate (1:10,000; Promega W401B) or anti-mouse IgG-HRP conjugate (1:10,000; Promega W402B) for 2 h rocking at room temperature. Blots were visualized using an Analytik Jena UVP ChemStudio and either SuperSignal West Pico PLUS Chemiluminescent Substrate, SuperSignal West Femto Chemiluminescent Substrate, or SuperSignal West Atto Chemiluminescent Substrate (ThermoFisher PI34580, PI34096, PIA38554).

Primary antibodies used, all at 1:1000 unless otherwise specified: anti-caspase-3 (Cell Signaling 9662), anti-cleaved-caspase-3 (Cell Signaling 9661), anti-caspase-8 (Cell Signaling 9746), anti-caspase-9 (Cell Signaling 9504), anti-PARP (Cell Signaling 9542), anti-FLIP (Cell Signaling 56343), anti-RIPK1 (Cell Signaling 3493), anti-phosphorylated-RIPK1 (Cell Signaling 53286), anti-RIPK3 (Cell Signaling 15828), anti-phosphorylated-RIPK3 (Cell Signaling 91702), anti-MLKL (Cell Signaling 37705), anti-phosphorylated-MLKL (Abcam ab196436), anti-actin (1:10,000; Sigma-Aldrich A5441).

Bacterial genome equivalents (GE) assay

To determine the bacterial load in BMDMs, cells were collected in 300 µL 1x PBS per 5 x 10^5 cells and transferred to 1.5 mL screw-cap microtubes containing 100 µL of 0.1 mm zirconia/silica beads (BioSpec Products 11079101z). Bacterial DNA was released by

457 homogenization three times at 5.0 m/s for 30 seconds using an MP Biosciences FastPrep-24,
458 followed by centrifugation for 1 minute at 12,000 rcf. DNA was quantified by spectrophotometer
459 (Biotek Cytation 3), and 50 ng of DNA diluted in molecular grade water was used for qPCR
460 quantification targeting the *C. burnetii dotA* gene.(29)
461
462 **Percent infection assay**
463 BMDMs were seeded at a density of $1x10^4$ cells/well in 96-well plates and infected with
464 mCherry-*C. burnetii* at an MOI of 100 GE/cell as described above. At 6 and 12 DPI, cells were
465 stained with Hoechst 33342 (2'-[4-ethoxyphenyl]-5-[4-methyl-1-piperazinyl]-2,5'-bi-1H-
466 benzimidazole) (Biorad 1351304). Using a Molecular Devices ImageXpress Micro Confocal, total
467 number of cells (Hoechst positive) and number of infected (mCherry positive) were counted, and
468 percent cell infection was computed.
469
470 **Cell viability assay**
471 BMDMs were seeded at a density of $1x10^4$ cells/well in 96-well plates and infected with
472 mCherry-*C. burnetii* at an MOI of 100 GE/cell as described above. At 6 and 12 DPI, cells were
473 stained with Hoechst 33342 (2'-[4-ethoxyphenyl]-5-[4-methyl-1-piperazinyl]-2,5'-bi-1H-
474 benzimidazole) (Biorad 1351304) and SYTOX green nucleic acid stain (Invitrogen/ThermoFisher
475 S7020). Using a Molecular Devices ImageXpress Micro Confocal, total number of cells (Hoechst
476 positive) and number of dead cells (SYTOX positive) were counted, and percent cell death was
477 computed.
478
479 **Quantitative real-time reverse transcription PCR (qRT-PCR)**
480 Total RNA was isolated from cells lysed in TRIzol (Invitrogen/ThermoFisher 15596026)
481 using the Direct-Zol RNA miniprep kit (Zymo research R2052) and cDNA was synthesized using
482 iScript Reverse Transcription Supermix (BioRad 1708840). qRT-qPCR was performed in triplicate

using single tube TaqMan assay (Invitrogen/ThermoFisher; Mm00443258_m1, Mm99999915_g1). For all gene expression data, *Gapdh* was used as an endogenous normalization control.

Enzyme-linked immunosorbent assay (ELISA)

BMDMs were seeded at a density of $2x10^5$ cells/well in 12-well plates and infected with mCherry-*C. burnetii* at an MOI of 300 GE/cell as described above. At 12 DPI, cell-free supernatants were collected from mock- and *C. burnetii*-infected cells. Supernatants were diluted with assay buffer and analyzed for presence of TNFα by ELISA (Invitrogen/ThermoFisher BMS607-3 or BMS607-2HS) according to manufacturer's protocol.

Statistical analyses

Densitometry was performed using ImageJ software. Statistical analyses were completed using GraphPad Prism 9. Statistical tests performed are specified in figure captions. Results shown are representative of at least three biological replicates from at least two independent experiments, as specified in the figure captions. Unless otherwise indicated, all error bars represent the standard deviation.

Author Contributions

Conceptualization by C. A. O. and A. G. G. Methodology by C. A. O., C. L., H. S. K., and A. G. G. Reagents provided by H. S. K. and A. G. G. Experiments, optimization, and statistics completed by C. A. O., C. L., and N. H. Figures made by C. A. O. in consultation with A. G. G. Writing by C. A. O. and revised by A. G. G., C. L., N. H., and H. S. K.

Acknowledgments

The *C. burnetii* clone 4 RSA439 used in this study was a gift from Dr. Robert A. Heinzen (Rocky Mountain Laboratories, NIH, Hamilton, MT). We thank Dr. Hongyan Guo and lab for supplying mutant mouse femurs for BMDM isolation, Dr. Santanu Bose and lab for supplying THP-1 cells, Miyoung Lee for experimental support, and Dr. Manish Chauhan for experimental support and technical expertise. This research was supported by NIH / National Institute of Allergy and Infectious Diseases (NIAID) grant R01 AI139051 to A. G. G and by a Poncin Fellowship to C.A.O.

Ethics Declarations

The authors declare no competing interests.

519 **References**

520 1. Davis GE, Cox HR, Parker RR, Dyer RE. 1938. A Filter-Passing Infectious Agent Isolated
521 from Ticks. Public Health Rep 1896-1970 53:2259–2282.

522 2. Derrick EH. 1983. “Q” Fever, a New Fever Entity: Clinical Features, Diagnosis and
523 Laboratory Investigation. Rev Infect Dis 5:790–800.

524 3. Eldin C, Mélenotte C, Mediannikov O, Ghigo E, Million M, Edouard S, Mege J-L, Maurin
525 M, Raoult D. 2017. From Q Fever to Coxiella burnetii Infection: a Paradigm Change. Clin
526 Microbiol Rev 30:115–190.

527 4. Raoult D, Marrie T, Mege J. 2005. Natural history and pathophysiology of Q fever. Lancet
528 Infect Dis 5:219–226.

529 5. Anderson A, Bijlmer H, Fournier P-E, Graves S, Hartzell J, Kersh GJ, Limonard G, Marrie
530 TJ, Massung RF, McQuiston JH, Nicholson WL, Paddock CD, Sexton DJ. 2013.
531 Diagnosis and management of Q fever--United States, 2013: recommendations from
532 CDC and the Q Fever Working Group. MMWR Recomm Rep Morb Mortal Wkly Rep
533 Recomm Rep 62:1–30.

534 6. Madariaga MG, Rezai K, Trenholme GM, Weinstein RA. 2003. Q fever: a biological
535 weapon in your backyard. Lancet Infect Dis 3:709–721.

536 7. Oyston PCF, Davies C. 2011. Q fever: the neglected biothreat agent. J Med Microbiol
537 60:9–21.

538 8. Morse SA, Quigley BR. 2020. Select agent regulations. Microb Forensics 425–439.

539 9. Maurin M, Raoult D. 1999. Q Fever. Clin Microbiol Rev 12:518–553.

10. Woldehiwet Z. 2004. Q fever (coxiellosis): epidemiology and pathogenesis. Res Vet Sci 77:93–100.

11. Brooke RJ, Kretzschmar MEE, Mutters NT, Teunis PF. 2013. Human dose response relation for airborne exposure to Coxiella burnetii. BMC Infect Dis 13:488.

12. Roest HIJ, Tilburg JJHC, van der Hoek W, Vellema P, van Zijderveld FG, Klaassen CHW, Raoult D. 2011. The Q fever epidemic in The Netherlands: history, onset, response and reflection. Epidemiol Infect 139:1–12.

13. Morroy G, Prins J, Bergevoet R, Schneeberger P, Bor HHJ, Hoek W van der, Hautvast J, Wijkmans CJ, Peters JB, Polder JJ. 2012. Of goats and humans; the societal costs of the Dutch Q fever saga. Int J Infect Dis 16:e266.

14. van der Hoek W, Morroy G, Renders NHM, Wever PC, Hermans MHA, Leenders ACAP, Schneeberger PM. 2012. Epidemic Q fever in humans in the Netherlands. Adv Exp Med Biol 984:329–364.

15. van Asseldonk MAPM, Prins J, Bergevoet RHM. 2013. Economic assessment of Q fever in the Netherlands. Prev Vet Med 112:27–34.

16. Sireci G, Badami GD, Di Liberto D, Blanda V, Grippi F, Di Paola L, Guercio A, de la Fuente J, Torina A. 2021. Recent Advances on the Innate Immune Response to Coxiella burnetii. Front Cell Infect Microbiol 11:754455.

17. Beare PA, Gilk SD, Larson CL, Hill J, Stead CM, Omsland A, Cockrell DC, Howe D, Voth DE, Heinzen RA. 2011. Dot/Icm type IVB secretion system requirements for Coxiella burnetii growth in human macrophages. mBio 2:e00175-00111.

18. Carey KL, Newton HJ, Lührmann A, Roy CR. 2011. The Coxiella burnetii Dot/Icm System Delivers a Unique Repertoire of Type IV Effectors into Host Cells and Is Required for Intracellular Replication. PLOS Pathog 7:e1002056.

19. Beare PA, Larson CL, Gilk SD, Heinzen RA. 2012. Two systems for targeted gene deletion in Coxiella burnetii. Appl Environ Microbiol 78:4580–4589.

20. Clemente TM, Mulye M, Justis AV, Nallandhighal S, Tran TM, Gilk SD. 2018. Coxiella burnetii Blocks Intracellular Interleukin-17 Signaling in Macrophages. Infect Immun 86:e00532-18.

21. Burette M, Allombert J, Lambou K, Maarifi G, Nisole S, Case EDR, Blanchet FP, Hassen-Khodja C, Cabantous S, Samuel J, Martinez E, Bonazzi M. 2020. Modulation of innate immune signaling by a Coxiella burnetii eukaryotic-like effector protein. Proc Natl Acad Sci 117:13708–13718.

22. Case EDR, Mahapatra S, Hoffpauir CT, Konganti K, Hillhouse AE, Samuel JE, Van Schaik EJ. 2022. Primary Murine Macrophages as a Tool for Virulence Factor Discovery in Coxiella burnetii. Microbiol Spectr 10:e02484-21.

23. Heinzen RA, Scidmore MA, Rockey DD, Hackstadt T. 1996. Differential interaction with endocytic and exocytic pathways distinguish parasitophorous vacuoles of Coxiella burnetii and Chlamydia trachomatis. Infect Immun 64:796–809.

24. Graham JG, Winchell CG, Kurten RC, Voth DE. 2016. Development of an Ex Vivo Tissue Platform To Study the Human Lung Response to Coxiella burnetii. Infect Immun 84:1438–1445.

582 25. Dragan AL, Kurten RC, Voth DE. 2019. Characterization of Early Stages of Human
583 Alveolar Infection by the Q Fever Agent Coxiella burnetii. Infect Immun 87:e00028-19.

584 26. Dragan AL, Voth DE. 2020. Coxiella burnetii: international pathogen of mystery. Microbes
585 Infect 22:100–110.

586 27. Capo C, Lindberg FP, Meconi S, Zaffran Y, Tardei G, Brown EJ, Raoult D, Mege J-L.
587 1999. Subversion of Monocyte Functions by Coxiella burnetii: Impairment of the Cross-
588 Talk Between αvβ3 Integrin and CR3. J Immunol 163:6078–6085.

589 28. McCaul TF, Williams JC. 1981. Developmental cycle of Coxiella burnetii: structure and
590 morphogenesis of vegetative and sporogenic differentiations. J Bacteriol 147:1063–1076.

591 29. Coleman SA, Fischer ER, Howe D, Mead DJ, Heinzen RA. 2004. Temporal Analysis of
592 Coxiella burnetii Morphological Differentiation. J Bacteriol 186:7344–7352.

593 30. Hackstadt T, Williams JC. 1981. Biochemical stratagem for obligate parasitism of
594 eukaryotic cells by Coxiella burnetii. Proc Natl Acad Sci 78:3240–3244.

595 31. Seshadri R, Paulsen IT, Eisen JA, Read TD, Nelson KE, Nelson WC, Ward NL, Tettelin
596 H, Davidsen TM, Beanan MJ, Deboy RT, Daugherty SC, Brinkac LM, Madupu R, Dodson
597 RJ, Khouri HM, Lee KH, Carty HA, Scanlan D, Heinzen RA, Thompson HA, Samuel JE,
598 Fraser CM, Heidelberg JF. 2003. Complete genome sequence of the Q-fever pathogen
599 Coxiella burnetii. Proc Natl Acad Sci 100:5455–5460.

600 32. Newton HJ, McDonough JA, Roy CR. 2013. Effector Protein Translocation by the Coxiella
601 burnetii Dot/Icm Type IV Secretion System Requires Endocytic Maturation of the
602 Pathogen-Occupied Vacuole. PLOS ONE 8:e54566.

603 33. Larson CL, Martinez E, Beare PA, Jeffrey B, Heinzen RA, Bonazzi M. 2016. Right on Q:
604 genetics begin to unravel *Coxiella burnetii* host cell interactions. Future Microbiol 11:919–
605 939.

606 34. Burette M, Bonazzi M. 2020. From neglected to dissected: How technological advances
607 are leading the way to the study of Coxiella burnetii pathogenesis. Cell Microbiol
608 22:e13180.

609 35. Lührmann A, Newton HJ, Bonazzi M. 2017. Beginning to Understand the Role of the
610 Type IV Secretion System Effector Proteins in Coxiella burnetii Pathogenesis. Curr Top
611 Microbiol Immunol 413:243–268.

612 36. Schulze-Luehrmann J, Liebler-Tenorio E, Felipe-López A, Lührmann A. 2023. Cell death
613 induction facilitates egress of Coxiella burnetii from infected host cells at late stages of
614 infection. Mol Microbiol https://doi.org/10.1111/mmi.15210.

615 37. Kerr JF, Wyllie AH, Currie AR. 1972. Apoptosis: a basic biological phenomenon with
616 wide-ranging implications in tissue kinetics. Br J Cancer 26:239–257.

617 38. Tang D, Kang R, Berghe TV, Vandenabeele P, Kroemer G. 2019. The molecular
618 machinery of regulated cell death. 5. Cell Res 29:347–364.

619 39. Pandian N, Kanneganti T-D. 2022. PANoptosis: A Unique Innate Immune Inflammatory
620 Cell Death Modality. J Immunol 209:1625–1633.

621 40. Elmore S. 2007. Apoptosis: A Review of Programmed Cell Death. Toxicol Pathol 35:495–
622 516.

623 41. Kroemer G, Galluzzi L, Brenner C. 2007. Mitochondrial Membrane Permeabilization in
624 Cell Death. Physiol Rev 87:99–163.

42. Li P, Nijhawan D, Budihardjo I, Srinivasula SM, Ahmad M, Alnemri ES, Wang X. 1997. Cytochrome c and dATP-dependent formation of Apaf-1/caspase-9 complex initiates an apoptotic protease cascade. Cell 91:479–489.

43. Riedl SJ, Salvesen GS. 2007. The apoptosome: signalling platform of cell death. Nat Rev Mol Cell Biol 8:405–413.

44. Schulze-Osthoff K, Ferrari D, Los M, Wesselborg S, Peter ME. 1998. Apoptosis signaling by death receptors. Eur J Biochem 254:439–459.

45. Hsu H, Xiong J, Goeddel DV. 1995. The TNF receptor 1-associated protein TRADD signals cell death and NF-kappa B activation. Cell 81:495–504.

46. Rothe M, Wong SC, Henzel WJ, Goeddel DV. 1994. A novel family of putative signal transducers associated with the cytoplasmic domain of the 75 kDa tumor necrosis factor receptor. Cell 78:681–692.

47. Micheau O, Tschopp J. 2003. Induction of TNF receptor I-mediated apoptosis via two sequential signaling complexes. Cell 114:181–190.

48. Newton K. 2015. RIPK1 and RIPK3: critical regulators of inflammation and cell death. Trends Cell Biol 25:347–353.

49. Nicholson DW, Thornberry NA. 1997. Caspases: killer proteases. Trends Biochem Sci 22:299–306.

50. Stennicke HR, Jürgensmeier JM, Shin H, Deveraux Q, Wolf BB, Yang X, Zhou Q, Ellerby HM, Ellerby LM, Bredesen D, Green DR, Reed JC, Froelich CJ, Salvesen GS. 1998. Pro-caspase-3 is a major physiologic target of caspase-8. J Biol Chem 273:27084–27090.

646 51. Taylor RC, Cullen SP, Martin SJ. 2008. Apoptosis: controlled demolition at the cellular
647 level. 3. Nat Rev Mol Cell Biol 9:231–241.

648 52. Varfolomeev EE, Schuchmann M, Luria V, Chiannilkulchai N, Beckmann JS, Mett IL,
649 Rebrikov D, Brodianski VM, Kemper OC, Kollet O, Lapidot T, Soffer D, Sobe T, Avraham
650 KB, Goncharov T, Holtmann H, Lonai P, Wallach D. 1998. Targeted Disruption of the
651 Mouse Caspase 8 Gene Ablates Cell Death Induction by the TNF Receptors, Fas/Apo1,
652 and DR3 and Is Lethal Prenatally. Immunity 9:267–276.

653 53. Oberst A, Dillon CP, Weinlich R, McCormick LL, Fitzgerald P, Pop C, Hakem R, Salvesen
654 GS, Green DR. 2011. Catalytic activity of the caspase-8–FLIPL complex inhibits RIPK3-
655 dependent necrosis. 7338. Nature 471:363–367.

656 54. Bertheloot D, Latz E, Franklin BS. 2021. Necroptosis, pyroptosis and apoptosis: an
657 intricate game of cell death. 5. Cell Mol Immunol 18:1106–1121.

658 55. Hitomi J, Christofferson DE, Ng A, Yao J, Degterev A, Xavier RJ, Yuan J. 2008.
659 Identification of a Molecular Signaling Network that Regulates a Cellular Necrotic Cell
660 Death Pathway. Cell 135:1311–1323.

661 56. Zhang D-W, Shao J, Lin J, Zhang N, Lu B-J, Lin S-C, Dong M-Q, Han J. 2009. RIP3, an
662 Energy Metabolism Regulator That Switches TNF-Induced Cell Death from Apoptosis to
663 Necrosis. Science 325:332–336.

664 57. He S, Wang L, Miao L, Wang T, Du F, Zhao L, Wang X. 2009. Receptor Interacting
665 Protein Kinase-3 Determines Cellular Necrotic Response to TNF-α. Cell 137:1100–1111.

58. Wang H, Sun L, Su L, Rizo J, Liu L, Wang L-F, Wang F-S, Wang X. 2014. Mixed Lineage Kinase Domain-like Protein MLKL Causes Necrotic Membrane Disruption upon Phosphorylation by RIP3. Mol Cell 54:133–146.

59. Osbron CA, Goodman AG. 2022. To die or not to die: Programmed cell death responses and their interactions with Coxiella burnetii infection. Mol Microbiol 0:1–20.

60. Lührmann A, Nogueira CV, Carey KL, Roy CR. 2010. Inhibition of pathogen-induced apoptosis by a Coxiella burnetii type IV effector protein. Proc Natl Acad Sci 107:18997–19001.

61. Eckart RA, Bisle S, Schulze-Luehrmann J, Wittmann I, Jantsch J, Schmid B, Berens C, Lührmann A. 2014. Antiapoptotic Activity of Coxiella burnetii Effector Protein AnkG Is Controlled by p32-Dependent Trafficking. Infect Immun 82:2763–2771.

62. Schäfer W, Eckart RA, Schmid B, Cagköylü H, Hof K, Muller YA, Amin B, Lührmann A. 2017. Nuclear trafficking of the anti-apoptotic *Coxiella burnetii* effector protein AnkG requires binding to p32 and Importin-α1: AnkG trafficking into the nucleus. Cell Microbiol 19:e12634.

63. Schäfer W, Schmidt T, Cordsmeier A, Borges V, Beare PA, Pechstein J, Schulze-Luehrmann J, Holzinger J, Wagner N, Berens C, Heydel C, Gomes JP, Lührmann A. 2020. The anti-apoptotic Coxiella burnetii effector protein AnkG is a strain specific virulence factor. Sci Rep 10:15396.

64. Bisle S, Klingenbeck L, Borges V, Sobotta K, Schulze-Luehrmann J, Menge C, Heydel C, Gomes JP, Lührmann A. 2016. The inhibition of the apoptosis pathway by the Coxiella burnetii effector protein CaeA requires the EK repetition motif, but is independent of survivin. Virulence 7:400–412.

689 65. Klingenbeck L, Eckart RA, Berens C, Lührmann A. 2013. The Coxiella burnetii type IV
690 secretion system substrate CaeB inhibits intrinsic apoptosis at the mitochondrial level.
691 Cell Microbiol 15:675–687.

692 66. Friedrich A, Beare PA, Schulze-Luehrmann J, Cordsmeier A, Pazen T, Sonnewald S,
693 Lührmann A. 2021. The Coxiella burnetii effector protein CaeB modulates endoplasmatic
694 reticulum (ER) stress signalling and is required for efficient replication in Galleria
695 mellonella. Cell Microbiol 23:e13305.

696 67. Voth DE, Howe D, Heinzen RA. 2007. Coxiella burnetii inhibits apoptosis in human THP-1
697 cells and monkey primary alveolar macrophages. Infect Immun 75:4263–4271.

698 68. Cordsmeier A, Wagner N, Lührmann A, Berens C. 2019. Defying Death – How Coxiella
699 burnetii Copes with Intentional Host Cell Suicide. Yale J Biol Med 92:619–628.

700 69. Kaiser WJ, Upton JW, Long AB, Livingston-Rosanoff D, Daley-Bauer LP, Hakem R,
701 Caspary T, Mocarski ES. 2011. RIP3 mediates the embryonic lethality of caspase-8-
702 deficient mice. 7338. Nature 471:368–372.

703 70. Berger SB, Kasparcova V, Hoffman S, Swift B, Dare L, Schaeffer M, Capriotti C, Cook M,
704 Finger J, Hughes-Earle A, Harris PA, Kaiser WJ, Mocarski ES, Bertin J, Gough PJ. 2014.
705 Cutting Edge: RIP1 Kinase Activity Is Dispensable for Normal Development but Is a Key
706 Regulator of Inflammation in SHARPIN-Deficient Mice. J Immunol 192:5476–5480.

707 71. Mandal P, Berger SB, Pillay S, Moriwaki K, Huang C, Guo H, Lich JD, Finger J,
708 Kasparcova V, Votta B, Ouellette M, King BW, Wisnoski D, Lakdawala AS, DeMartino
709 MP, Casillas LN, Haile PA, Sehon CA, Marquis RW, Upton J, Daley-Bauer LP, Roback L,
710 Ramia N, Dovey CM, Carette JE, Chan FK-M, Bertin J, Gough PJ, Mocarski ES, Kaiser

WJ. 2014. RIP3 Induces Apoptosis Independent of Pronecrotic Kinase Activity. Mol Cell 56:481–495.

72. Orning P, Lien E. 2020. Multiple roles of caspase-8 in cell death, inflammation, and innate immunity. J Leukoc Biol JLB.3MR0420-305R.

73. Dondelinger Y, Jouan-Lanhouet S, Divert T, Theatre E, Bertin J, Gough PJ, Giansanti P, Heck AJR, Dejardin E, Vandenabeele P, Bertrand MJM. 2015. NF-κB-Independent Role of IKKα/IKKβ in Preventing RIPK1 Kinase-Dependent Apoptotic and Necroptotic Cell Death during TNF Signaling. Mol Cell 60:63–76.

74. Peterson LW, Philip NH, DeLaney A, Wynosky-Dolfi MA, Asklof K, Gray F, Choa R, Bjanes E, Buza EL, Hu B, Dillon CP, Green DR, Berger SB, Gough PJ, Bertin J, Brodsky IE. 2017. RIPK1-dependent apoptosis bypasses pathogen blockade of innate signaling to promote immune defense. J Exp Med 214:3171–3182.

75. Xu D, Jin T, Zhu H, Chen H, Ofengeim D, Zou C, Mifflin L, Pan L, Amin P, Li W, Shan B, Naito MG, Meng H, Li Y, Pan H, Aron L, Adiconis X, Levin JZ, Yankner BA, Yuan J. 2018. TBK1 Suppresses RIPK1-Driven Apoptosis and Inflammation during Development and in Aging. Cell 174:1477-1491.e19.

76. Dellacasagrande J, Capo C, Raoult D, Mege J-L. 1999. IFN-γ-Mediated Control of Coxiella burnetii Survival in Monocytes: The Role of Cell Apoptosis and TNF. J Immunol 162:2259–2265.

77. Dellacasagrande J, Ghigo E, Raoult D, Capo C, Mege J-L. 2002. IFN-γ-Induced Apoptosis and Microbicidal Activity in Monocytes Harboring the Intracellular Bacterium Coxiella burnetii Require Membrane TNF and Homotypic Cell Adherence. J Immunol 169:6309–6315.

734 78. Bradley WP, Boyer MA, Nguyen HT, Birdwell LD, Yu J, Ribeiro JM, Weiss SR, Zamboni
735 DS, Roy CR, Shin S. 2016. Primary Role for Toll-Like Receptor-Driven Tumor Necrosis
736 Factor Rather than Cytosolic Immune Detection in Restricting Coxiella burnetii Phase II
737 Replication within Mouse Macrophages. Infect Immun 84:998–1015.

738 79. Mauermeir M, Ölke M, Hayek I, Schulze-Luehrmann J, Dettmer K, Oefner PJ, Berens C,
739 Menge C, Lührmann A. 2023. Bovine blood derived macrophages are unable to control
740 Coxiella burnetii replication under hypoxic conditions. Front Immunol 14:960927.

741 80. Graham JG, MacDonald LJ, Hussain SK, Sharma UM, Kurten RC, Voth DE. 2013.
742 Virulent Coxiella burnetii pathotypes productively infect primary human alveolar
743 macrophages. Cell Microbiol 15:1012–1025.

744 81. Cunha LD, Ribeiro JM, Fernandes TD, Massis LM, Khoo CA, Moffatt JH, Newton HJ, Roy
745 CR, Zamboni DS. 2015. Inhibition of inflammasome activation by Coxiella burnetii type IV
746 secretion system effector IcaA. 1. Nat Commun 6:10205.

747 82. Delaney MA, Hartigh A den, Carpentier SJ, Birkland TP, Knowles DP, Cookson BT,
748 Frevert CW. 2021. Avoidance of the NLRP3 Inflammasome by the Stealth Pathogen,
749 Coxiella burnetii. Vet Pathol 58:624–642.

750 83. Boyer MA, Fischer NL, Shin S. 2023. TNF and type I IFN induction of the IRG1-itaconate
751 pathway restricts Coxiella burnetii replication within mouse macrophages. bioRxiv
752 https://doi.org/10.1101/2023.07.07.548079.

753 84. Kohl L, Siddique MNAA, Bodendorfer B, Berger R, Preikschat A, Daniel C, Ölke M,
754 Liebler-Tenorio E, Schulze-Luehrmann J, Mauermeir M, Yang K, Hayek I, Szperlinski M,
755 Andrack J, Schleicher U, Bozec A, Krönke G, Murray PJ, Wirtz S, Yamamoto M, Schatz
756 V, Jantsch J, Oefner P, Degrandi D, Pfeffer K, Mertens-Scholz K, Rauber S, Bogdan C,

Dettmer K, Lührmann A, Lang R. 2023. Macrophages inhibit Coxiella burnetii by the ACOD1-itaconate pathway for containment of Q fever. EMBO Mol Med 15:e15931.

85. Andoh M, Zhang G, Russell-Lodrigue KE, Shive HR, Weeks BR, Samuel JE. 2007. T Cells Are Essential for Bacterial Clearance, and Gamma Interferon, Tumor Necrosis Factor Alpha, and B Cells Are Crucial for Disease Development in Coxiella burnetii Infection in Mice. Infect Immun 75:3245–3255.

86. Schoffelen T, Kampschreur LM, van Roeden SE, Wever PC, den Broeder AA, Nabuurs-Franssen MH, Sprong T, Joosten L a. B, van Riel PLCM, Oosterheert JJ, van Deuren M, Creemers MCW. 2014. Coxiella burnetii infection (Q fever) in rheumatoid arthritis patients with and without anti-TNFα therapy. Ann Rheum Dis 73:1436–1438.

87. van der Hoek W, Versteeg B, Meekelenkamp JCE, Renders NHM, Leenders ACAP, Weers-Pothoff I, Hermans MHA, Zaaijer HL, Wever PC, Schneeberger PM. 2011. Follow-up of 686 patients with acute Q fever and detection of chronic infection. Clin Infect Dis Off Publ Infect Dis Soc Am 52:1431–1436.

88. Fischer R, Kontermann RE, Pfizenmaier K. 2020. Selective Targeting of TNF Receptors as a Novel Therapeutic Approach. Front Cell Dev Biol 8.

89. Ghigo E, Capo C, Amirayan N, Raoult D, Mege J. 2000. The 75-kD tumour necrosis factor (TNF) receptor is specifically up-regulated in monocytes during Q fever endocarditis. Clin Exp Immunol 121:295–301.

90. Weng D, Marty-Roix R, Ganesan S, Proulx MK, Vladimer GI, Kaiser WJ, Mocarski ES, Pouliot K, Chan FK-M, Kelliher MA, Harris PA, Bertin J, Gough PJ, Shayakhmetov DM, Goguen JD, Fitzgerald KA, Silverman N, Lien E. 2014. Caspase-8 and RIP kinases

regulate bacteria-induced innate immune responses and cell death. Proc Natl Acad Sci 111:7391–7396.

91. Philip NH, Dillon CP, Snyder AG, Fitzgerald P, Wynosky-Dolfi MA, Zwack EE, Hu B, Fitzgerald L, Mauldin EA, Copenhaver AM, Shin S, Wei L, Parker M, Zhang J, Oberst A, Green DR, Brodsky IE. 2014. Caspase-8 mediates caspase-1 processing and innate immune defense in response to bacterial blockade of NF-κB and MAPK signaling. Proc Natl Acad Sci 111:7385–7390.

92. Sarhan J, Liu BC, Muendlein HI, Li P, Nilson R, Tang AY, Rongvaux A, Bunnell SC, Shao F, Green DR, Poltorak A. 2018. Caspase-8 induces cleavage of gasdermin D to elicit pyroptosis during Yersinia infection. Proc Natl Acad Sci 115:E10888–E10897.

93. Orning P, Weng D, Starheim K, Ratner D, Best Z, Lee B, Brooks A, Xia S, Wu H, Kelliher MA, Berger SB, Gough PJ, Bertin J, Proulx MM, Goguen JD, Kayagaki N, Fitzgerald KA, Lien E. 2018. Pathogen blockade of TAK1 triggers caspase-8–dependent cleavage of gasdermin D and cell death. Science 362:1064–1069.

94. Musarra-Pizzo M, Pennisi R, Lombardo D, Velletri T, Sciortino MT. 2022. Direct cleavage of caspase-8 by herpes simplex virus 1 tegument protein US11. 1. Sci Rep 12:12317.

95. Guo H, Koehler HS, Mocarski ES, Dix RD. 2022. RIPK3 and caspase 8 collaborate to limit herpes simplex encephalitis. PLoS Pathog 18:e1010857.

96. Marino-Merlo F, Klett A, Papaianni E, Drago SFA, Macchi B, Rincón MG, Andreola F, Serafino A, Grelli S, Mastino A, Borner C. 2023. Caspase-8 is required for HSV-1-induced apoptosis and promotes effective viral particle release via autophagy inhibition. 4. Cell Death Differ 30:885–896.

97. Meinzer U, Barreau F, Esmiol-Welterlin S, Jung C, Villard C, Léger T, Ben-Mkaddem S, Berrebi D, Dussaillant M, Alnabhani Z, Roy M, Bonacorsi S, Wolf-Watz H, Perroy J, Ollendorff V, Hugot J-P. 2012. Yersinia pseudotuberculosis effector YopJ subverts the Nod2/RICK/TAK1 pathway and activates caspase-1 to induce intestinal barrier dysfunction. Cell Host Microbe 11:337–351.

98. Mittal R, Peak-Chew S-Y, McMahon HT. 2006. Acetylation of MEK2 and IκB kinase (IKK) activation loop residues by YopJ inhibits signaling. Proc Natl Acad Sci 103:18574–18579.

99. Mukherjee S, Keitany G, Li Y, Wang Y, Ball HL, Goldsmith EJ, Orth K. 2006. Yersinia YopJ Acetylates and Inhibits Kinase Activation by Blocking Phosphorylation. Science 312:1211–1214.

100. Paquette N, Conlon J, Sweet C, Rus F, Wilson L, Pereira A, Rosadini CV, Goutagny N, Weber ANR, Lane WS, Shaffer SA, Maniatis S, Fitzgerald KA, Stuart L, Silverman N. 2012. Serine/threonine acetylation of TGFβ-activated kinase (TAK1) by Yersinia pestis YopJ inhibits innate immune signaling. Proc Natl Acad Sci 109:12710–12715.

101. Omsland A, Cockrell DC, Howe D, Fischer ER, Virtaneva K, Sturdevant DE, Porcella SF, Heinzen RA. 2009. Host cell-free growth of the Q fever bacterium Coxiella burnetii. Proc Natl Acad Sci 106:4430–4434.

102. Omsland A, Beare PA, Hill J, Cockrell DC, Howe D, Hansen B, Samuel JE, Heinzen RA. 2011. Isolation from Animal Tissue and Genetic Transformation of Coxiella burnetii Are Facilitated by an Improved Axenic Growth Medium. Appl Environ Microbiol 77:3720–3725.

103. Sanchez SE, Vallejo-Esquerra E, Omsland A. 2018. Use of Axenic Culture Tools to Study Coxiella burnetii. Curr Protoc Microbiol 50:e52.

824 104. Brennan RE, Samuel JE. 2003. Evaluation of Coxiella burnetii antibiotic susceptibilities by
825 real-time PCR assay. J Clin Microbiol 41:1869–1874.

826

827

Figure Captions

Figure 1. *C. burnetii* inhibition of caspase-8 activation and extrinsic apoptosis. THP-1 cells were differentiated using 100 nM PMA and infected with an mCherry-expressing Nine Mile Phase II (NMII) strain of *C. burnetii* (mCherry-*C. burnetii*) at MOI 25 GE/cell. At 3 DPI, cells were pre-treated with 10 µg/mL CHX for 4 h followed by overnight treatment with 20 ng/mL TNFα. (A) Representative images taken at 40x magnification. (B) Western blotting of samples as indicated. (C) Densitometry was completed in ImageJ and significance was determined by one-way ANOVA with Šídák's multiple comparisons test. Data are representative of three biological replicates from three independent experiments. *p < 0.05, **p < 0.01, ***p < 0.001, ****p < 0.0001

Figure 2. Necroptosis exacerbation by *C. burnetii* infection. L929 cells were infected with mCherry-*C. burnetii* at MOI 300 GE/cell. At 3 and 6 DPI, cells were pre-treated with 50 µM Z-VAD-FMK for 30 mins followed by 3 h incubation with 20 ng/mL TNFα. (A,D) Representative 3 and 6 DPI images taken at 40x magnification. (B,E) Western blotting of samples as indicated. (C,F) Densitometry was completed in ImageJ and significance was determined by paired t-test. Data are representative of four biological replicates from four independent experiments. *p < 0.05, **p < 0.01, ***p < 0.001, ****p < 0.0001

Figure 3. Caspase-8 restricts *C. burnetii* replication and spread. Primary murine bone marrow-derived macrophages (BMDMs) (C57B6J WT, *Ripk1*$^{K45A/K45A}$, *Ripk3*$^{K51A/K51A}$, and *Casp8*$^{-/-}$ *Ripk3*$^{K51A/K51A}$) were infected with mCherry-*C. burnetii* at MOI 100 GE/cell. At 3, 6, 9, and 12 DPI, cells were imaged and lysed using a MP Biosciences FastPrep-24 machine and 0.1 mm zirconia beads. (A) Representative 12 DPI images taken at 40x magnification. (B) Quantification of *C. burnetii* genome equivalents (GE) as determined by *DotA* qPCR performed on whole cell

lysates. Significance was determined by mixed effects analysis with Tukey's multiple comparisons test. Data are representative of three biological replicates from three independent experiments. Error bars in (B) represent SEM instead of SD. (C) Percent infection was measured at 6 and 12 DPI using a Molecular Devices ImageXpress Micro Confocal. Data represents 6 biological replicates, and 6 and 12 DPI datasets are from two independent experiments. Significance was determined by two-way ANOVA with Tukey's multiple comparisons test. *p < 0.05, **p < 0.01, ***p < 0.001, ****p < 0.0001

Figure 4. BMDMs lacking RIPK3 or RIPK3 and caspase-8 activity have decreased cytotoxicity throughout *C. burnetii* infection. BMDMs were infected with mCherry-*C. burnetii* as in Fig 3. At 6 DPI (A) and at 12 DPI (B), cytotoxicity was measured by SYTOX staining using a Molecular Devices ImageXpress Micro Confocal. Data are representative of four-six biological replicates from two independent experiments. Percent SYTOX positive was normalized to the average mock cytotoxicity within genotypes and significance was determined by two-way ANOVA with Tukey's multiple comparisons test. *p < 0.05, **p < 0.01, ***p < 0.001, ****p < 0.0001

Figure 5. TNFα production is reduced in caspase-8$^{-/-}$ BMDMs during *C. burnetii* infection. BMDMs were infected with mCherry-*C. burnetii* as in Fig 3. (A) Relative expression of *tnfa* at 12 DPI was determined by qRT-PCR. Ct values were normalized first to *gapdh* expression, then to mock-infected samples. Data are representative of three biological replicates from three independent experiments, and significance was determined by two-way ANOVA with Tukey's multiple comparisons test. (B) Quantification of TNFα at 12 DPI in cell-free supernatant. TNFα pg/mL concentrations were normalized to the average mock values within genotypes. Data are representative of seven biological replicates from two independent experiments. Significance was

877 determined by two-way ANOVA with Tukey's multiple comparisons test. *p < 0.05, **p < 0.01, ***p

878 < 0.001, ****p < 0.0001

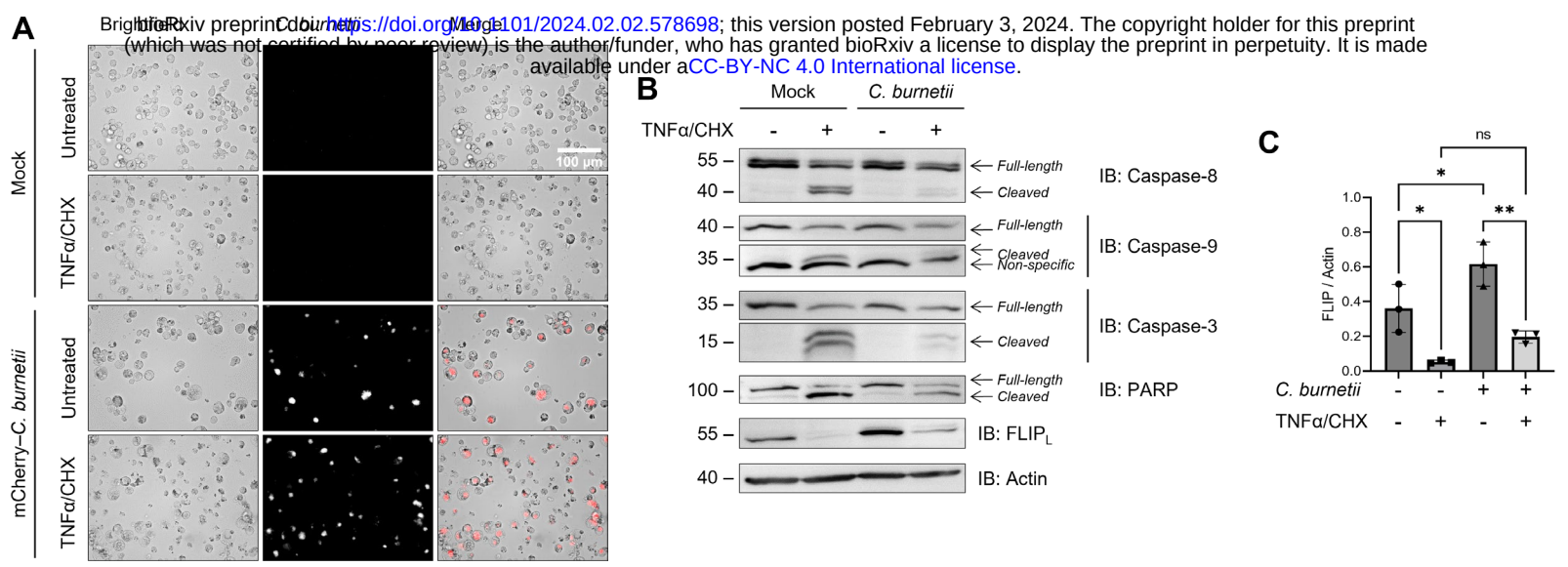

Figure 1. *C. burnetii* inhibition of caspase-8 activation and extrinsic apoptosis. THP-1 cells were differentiated using 100nM PMA and infected with an mCherry-expressing Nine Mile Phase II (NMII) strain of *C. burnetii* (mCherry-*C. burnetii*) at MOI 25. At 3 DPI, cells were pre-treated with 10 µg/mL CHX for 4 hrs followed by overnight treatment with 20 ng/mL TNFα. (A) Representative images taken at 40x magnification. (B) Western blotting of samples as indicated. (C) Densitometry was completed in ImageJ and significance was determined by one-way ANOVA with Šídák's multiple comparisons test. Data is representative of 3 biological replicates from 3 independent experiments. *p < 0.05, **p < 0.01, ***p < 0.001, ****p < 0.0001

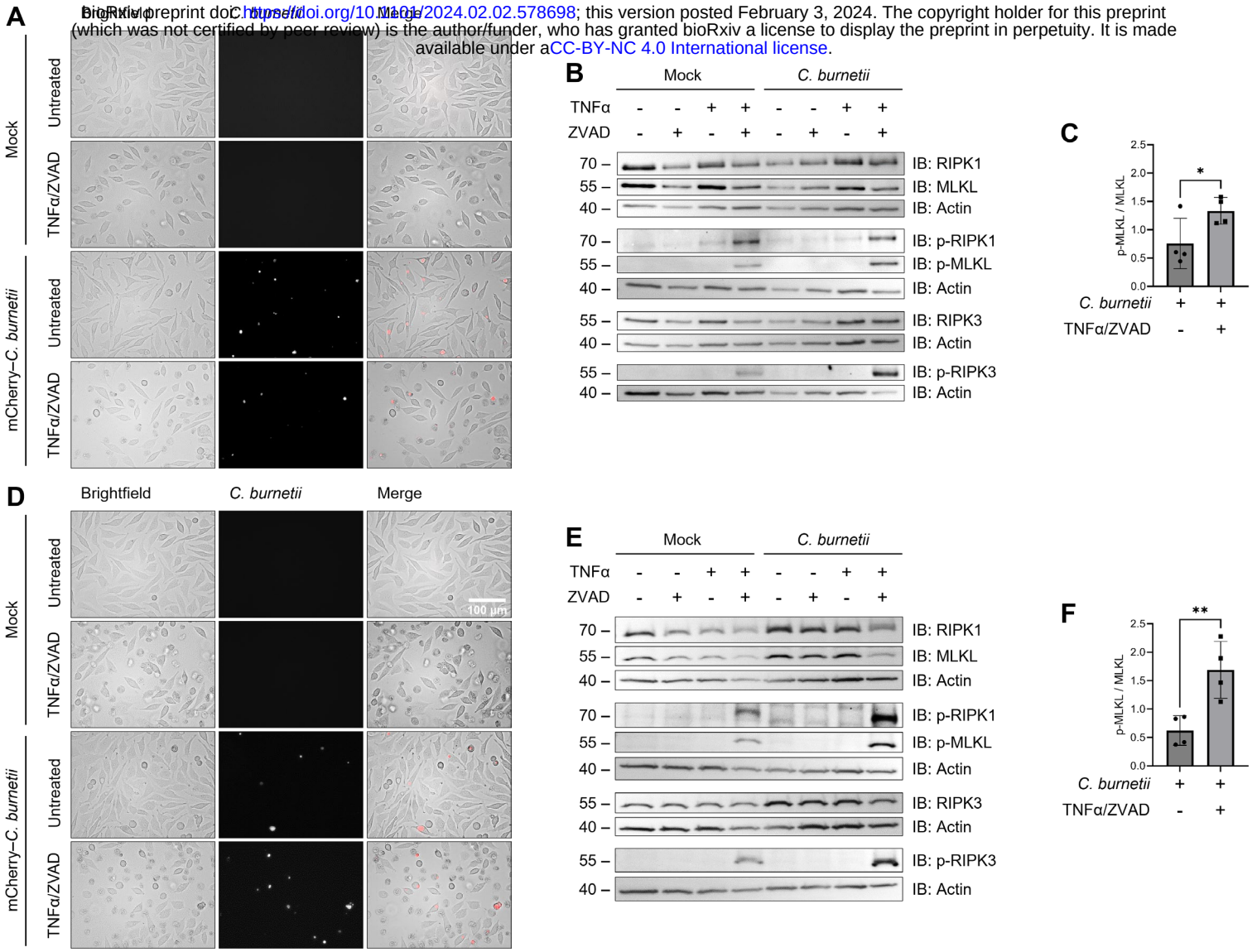

Figure 2. Necroptosis exacerbation by *C. burnetii* infection. L929 cells were infected with mCherry-*C. burnetii* at MOI 300. At 3 and 6 DPI, cells were pre-treated with 50 μM Z-VAD-FMK for 30 mins followed by 3 hrs incubation with 20 ng/mL TNFα. (A,D) Representative 3 and 6 DPI images taken at 40x magnification. (B,E) Western blotting of samples as indicated. (C,F) Densitometry was completed in ImageJ and significance was determined by paired t-test. Data is representative of 4 biological replicates from 4 independent experiments. *p < 0.05, **p < 0.01, ***p < 0.001, ****p < 0.0001

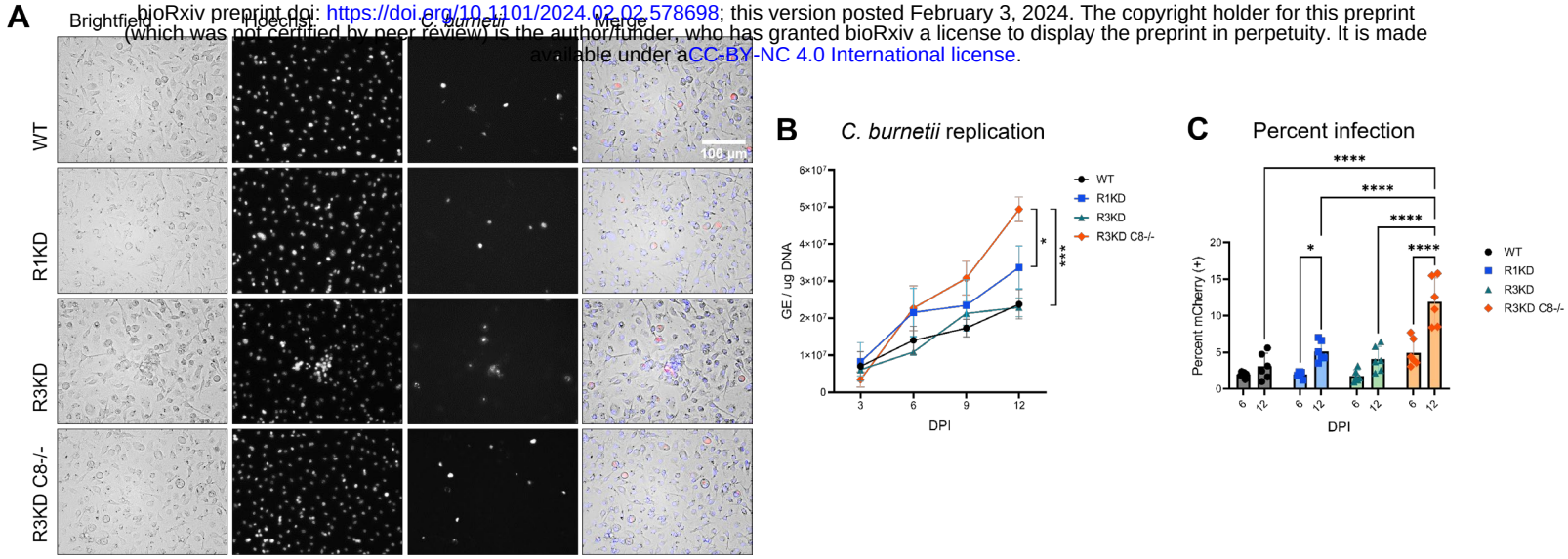

Figure 3. Caspase-8 restricts *C. burnetii* replication and spread. Primary murine bone marrow-derived macrophages (BMDMs) (C57B6J WT, *Ripk1*$^{K45A/K45A}$, *Ripk3*$^{K51A/K51A}$, and *Ripk3*$^{K51A/K51A}$*Casp8*$^{-/-}$) were infected with mCherry-*C. burnetii* at MOI 100. At 3, 6, 9, and 12 DPI, cells were imaged and lysed using a MP Biosciences FastPrep-24 machine and 0.1 mm zirconia beads. (A) Representative 12 DPI images taken at 40x magnification. (B) Quantification of *C. burnetii* genome equivalents (GE) as determined by *DotA* qPCR performed on whole cell lysates. Significance was determined by mixed effects analysis with Tukey's multiple comparisons test. Data represents 3 biological replicates from 3 independent experiments. Error bars in (B) represent SEM instead of SD. (C) Percent infection was measured at 6 and 12 DPI using a Molecular Devices ImageXpress Micro Confocal. Data represents 6 biological replicates, and 6 and 12 DPI datasets are from 2 independent experiments. Significance was determined by two-way ANOVA with Tukey's multiple comparisons test. *p < 0.05, **p < 0.01, ***p < 0.001, ****p < 0.0001

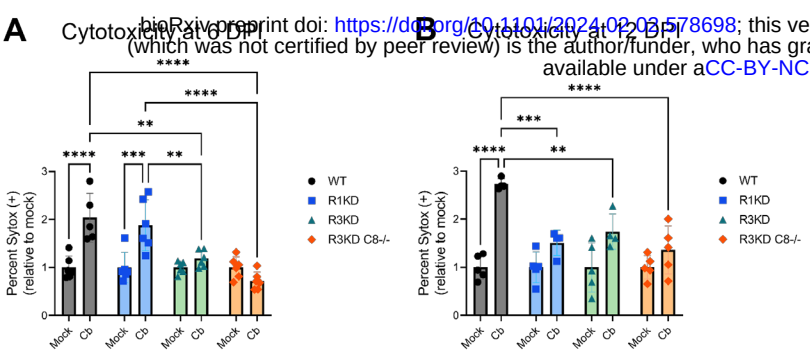

Figure 4. BMDMs lacking RIPK3 or RIPK3 and caspase-8 activity have decreased cytotoxicity throughout *C. burnetii* infection. BMDMs were infected with mCherry-*C. burnetii* as in Fig 3. At 6 DPI (A) and at 12 DPI (B), cytotoxicity was measured by sytox staining using a Molecular Devices ImageXpress Micro Confocal. Data represents 4-6 biological replicates, and 6 and 12 DPI datasets are from 2 independent experiments. Percent sytox positive was normalized to the average mock cytotoxicity within genotypes and significance was determined by two-way ANOVA with Tukey's multiple comparisons test. *p < 0.05, **p < 0.01, ***p < 0.001, ****p < 0.0001

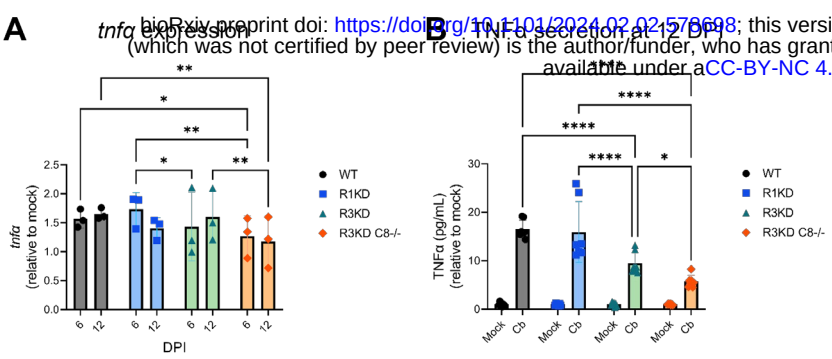

Figure 5. TNFα production is reduced in caspase-8$^{-/-}$ BMDMs during *C. burnetii* infection. BMDMs were infected with mCherry-*C. burnetii* as in Fig 3. (A) Relative expression of *tnfa* at 12 DPI was determined by qRT-PCR. Ct values were normalized first to *gapdh* expression, then to mock-infected samples. Data represents 3 biological replicates from three independent experiments, and significance was determined by two-way ANOVA with Tukey's multiple comparisons test. (B) Quantification of TNFα at 12 DPI in cell-free supernatant. TNFα pg/mL concentrations were normalized to the average mock values within genotypes. Data represents 7 biological replicates from 2 independent experiments. Significance was determined by two-way ANOVA with Tukey's multiple comparisons test. *p < 0.05, **p < 0.01, ***p < 0.001, ****p < 0.0001